第33卷第4期
2014年8月

红外与毫米波学报
J. Infrared Millim. Waves

Vol. 33, No. 4
August, 2014

文章编号:1001-9014(2014)04-0344-05

DOI:10.3724/SP.J.1010.2014.00344

Plasmon antenna at mid-infrared made by metallic apertures

YANG Li, WANG Bin, CAO Ling-Ling, YE Yong-Hong*

(Jiangsu Key Lab on Opto-Eelectronic Technology,
School of Physical Science and Technology, Nanjing Normal University, Nanjing 210023, China)

Abstract: The transmission spectra and far-field radiation patterns of periodic metallic aperture arrays are studied in mid-infrared region. We find that the samples have two transmission bands in mid-infrared region. The central positions of transmission bands red-shifts with the increase of the hole-diameter or the lattice constant. The periodic metallic aperture arrays can behave as electrical dipole arrays at the central positions of the transmission bands. The radiation intensity in far-field is strong at the two frequencies. The intensity increase with the decrease of the hole diameter or the increase of the lattice constant.

Key words: far-field radiation, metallic apertures, mid-infrared, dipole arrays, surface plasmon polariton
PACS: 42.25.Bs, 52.35.Hr, 41.20.Jb, 73.21.Ac

基于中红外波段的等离子体金属孔天线

杨 理, 王 斌, 曹玲玲, 叶永红*
(南京师范大学 物理科学与技术学院,江苏 南京 210023)

摘要:研究了周期性金属孔阵列的光学和远场辐射特性,实验发现所有样品在中红外波段都有两个透射峰,当金属孔径或者孔阵的晶格常数变大时,透过峰的中心频率发生红移.在透过率的中心频率附近,周期性的金属孔阵列表现出偶极子阵列的特性,其远场辐射特性随着孔径的减小或者孔阵列晶格常数的增大而增强.

关 键 词:远场辐射;金属孔阵;中红外;偶极子阵列;表面等离激元

中图分类号:O439 **文献标识码**:A

Introduction

Antennas have attracted a lot of attentions due to their wide applications in millimeter-waves and microwaves over the past decades. Recently, antennas in optical frequency region have sparked great interests for their potential applications[1-5]. Most researches on optical antennas are based on wire antennas (metal particles) or nanorods arrays[6-7], such as bow-tie antennas[8-9], Yagi-Uda antennas[10-13], log-periodic antennas[14], spherical nano-antennas[15-17], etc. Slot antennas (metallic apertures), the complementary structure of wire antennas, have the advantages of robustness and greater control of the radiation pattern in microwave region. In optical region, numerous researches have been done on aperture arrays[18-21], such as the extraordinary optical transmission (EOT) phenomena[22-26] of metallic apertures, which originates from both the surface plasmon polaritons (SPPs) and the local surface plasmon polaritons (LSPPs)[27]. Guo *et al.* have reported the bow-tie slot antennas with two types of resonances in the near infrared and visible spectral range[28]. It has been found that gold bow-tie shaped aperture nano-antenna has a localized enhanced field which can improve the resolution of the microscopy and optical lithography[29]. U-T-shaped nano-aperture antennas are reported to have multiple resonant bands[30]. Moreover, Peng *et al.* have reported that a metallic aperture array performs as an optical antenna array, and the far-field emission is originated from plasmonic emission[31]. Studies in EOT phenomena indicate that dipole moments will be induced at the edge of the metallic apertures at the position of the transmission peak when illuminated by a plane wave[31]. However, whether the far-field radiation patterns can be modulated by the induced local electric field has not been studied.

In this paper, we experimentally fabricate the periodic metallic aperture arrays by using optical lithography

Received date: 2013-04-24, **revised date**: 2014-05-29 收稿日期:2013-04-24, 修回日期:2014-05-29
Foundation items: Supported by the Specialized Research Fund for the Doctoral Program of Higher Education of China(20093207110012)
Biography: YANG Li (1989-), female, Xuzhou, China, Master. Research fields include nano-photonics. E-mail: s989757@126.com
* **Corresponding author**: E-mail: yeyonghong@ninu.edu.cn

and analyze the sample's transmission spectra and far-field radiation patterns. The results suggest that all the samples have two transmission bands in the mid-infrared frequency. The intensities and central positions of transmission bands depend on the diameter and lattice constant of the aperture arrays. The near-field responses at the central positions of transmission bands suggest that each metal aperture behaves as one electrical dipole at the central position of the transmission bands. The far-field patterns indicate that the metal aperture arrays behave well as electrical dipole arrays.

1 Experimental results

The samples consist of one silver layer and one SU－8 layer, and the two layers are perforated with a square array of circular apertures. The thickness of silver layer (h) and SU－8 layer (H) is 50 nm and 2 μm, respectively. The detailed fabrication procedures can be found in our previous publication[33]. In this experiment, we fabricated three samples: samples A, B and C. The diameter of the holes (m) is 5, 5 and 6 μm, and the lattice constant (n) is 9, 10 and 10 μm for samples A, B and C, respectively. The JEOL JSM－5610LV scanning electronic microscope (SEM) image of sample B is shown in Fig. 1(a). The schematic of a unit cell of our sample is shown in Fig. 1(b), which also shows the characters of the incident light. The transmission spectra of the samples were measured with TE incident light at normal incidence by using a Bruker Optics Equinox 55 Fourier transform IR spectrometer.

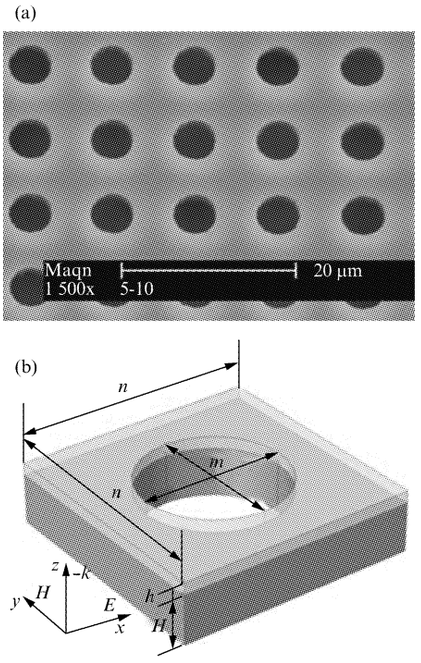

Fig. 1 (a) SEM image of sample B, (b) schematic diagram of one unit cell of our samples. The diameter (m) and lattice (n) constant are indicated. The propagation and polarization directions are indicated

图1 (a) 样品B的SEM图,(b)样品单元示意图,金属孔径是m,孔阵周期是n,图中已标出电场和磁场的传播和偏振方向

2 Simulation results

We used a numerical simulator, Comsol Multiphysics, to calculate the transmission and the far-field patterns of all samples. This simulator is a popular commercial finite-element-based electromagnetic (FEM) solver. When calculating the transmission, we built a 3D model with a unit cell shown in Fig. 1(b). The incident light has the same polarization and propagation directions as those used in the experiment. The incident light propagates along the-z direction and its electric field is polarized along the x direction and its magnetic field is polarized along the y direction. To simulate an infinite array, we defined one pair of perfect electrical conductor boundaries of each unit cell along the polarized direction of electric field (x direction in this case), and the other pair of boundaries is perfect magnetic conductor along the magnetic field (y direction in this case). When calculating the far-field patterns, we built a 3D model with a finite 4×4 unit cell array. The relative dielectric constant of SU－8 is assumed to be $2.56 + i * 0.05$[31]. The relative dielectric constant of silver is taken from Ref. 33.

Figure 2(a) is the experimental transmission spectra of the samples. As shown in Fig. 2(a), there are two transmission bands (a higher frequency (HF) band and a lower frequency (LF) band) in the mid-infrared for the three samples. The central positions of the LF and HF bands are listed in Table 1. As shown in Table 1, both the HF and LF bands redshift when the lattice constant of the sample increases from 9 to 10 μm with a fixed hole-diameter of 5 μm. At a fixed lattice constant of 10 μm, the two bands also redshift slightly when the diameter of the sample increases from 5 to 6 μm. Figure 2(b) shows the caculated transmission spectra of the samples. As shown in Fig. 2(b), the simulated results match with experimental ones well, including the positions of two transmission bands and the redshift trend. The discrepancies between the measured spectra and the calculated ones are caused by the unavoidable inaccuracy when fabricating experimental samples. Moreover, the inaccuracy of material's dielectric loss between actual and ideal also results in the discrepancies.

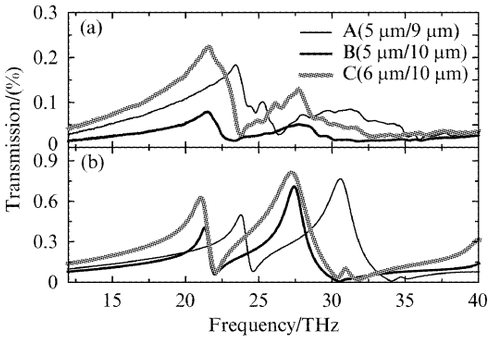

Fig. 2 (a) Measured transmission spectra of samples A, B and C, respectively. (b) Calculated transmission spectra of samples A, B and C, respectively

图2 (a) 样品A、B和C透射谱实验值,(b) 样品A、B和C透射谱仿真值

To study the far-field radiation properties, we swept the frequencies from 5 to 60 THz with a step size of 0.05 THz in the calculation. it was found that the radiation intensity in far-field is strong at the two frequencies. The frequency corresponding to the strong radiation intensity (SRIF) matches the central position of the transmission bands. Table 1 also lists the position of the SRIF. As shown in Table 1, the position of SRIF redshifts when the lattice constant of the sample increases from 9 to 10 μm with a fixed diameter of 5 μm. At a fixed lattice constant of 10 μm, the position of the SRIF also shows slightly redshift when the diameter of the sample increases from 5 to 6 μm. In summary, the SRIFs will redshift with the redshift of the transmission peaks. The little inconsistent between the position of the SRIF and the position of the transmission peak is due to the following reason: the transmissions are obtained from an infinite aperture array, while the antenna directivities are obtained from a finite plane, namely a finite 4×4 array.

Table 1 Central positions of the transmission band and SRIFs

表1 透过率和SRIFs的中心频率

Sample	Transmission peak/THz (experiment)		Transmission peak/THz (simulation)		Antenna (SRIFs)/THz	
	LF	HF	LF	HF	LF	HF
A	23.44	31.15	23.79	30.55	22.5	31
B	21.58	27.82	21.22	27.36	20.5	28
C	21.52	27.82	21.07	27.28	20	28

There are also relations between the intensity of transmission peaks and the far-field maximum radiation intensity. The antenna's radiation patterns at the lower SRIF and higher SRIF are shown in Fig. 3(a) and Fig. 3(b), respectively. The antenna's radiation patterns at the two frequencies have some similar properties. First, the transmission intensity of sample A is stronger than that of sample B, while the antenna's radiation intensity of sample B is much stronger than that of sample A. Second, the transmission intensity of sample C is stronger than that of sample B, while the antenna's radiation intensity of sample B is much stronger than that of sample C. Consequently, the antenna's radiation intensity of sample B is the strongest of the three samples at both the central position of the lower and higher SRIF.

3 Theoretical analysis

To study the relation of the frequency of the position between the SRIFs and the EOT pass bands, we have calculated the electric field distribution and the electric displacement vector in the aperture array at the central frequencies of HF and LF bands. As shown in Fig. 4, when excited by plane wave, the electric field at the edge of each aperture is much stronger than that at other regions. The electric displacement vector is along the electric field (along the x axis). The charge density accumulated at opposite sides of the aperture along the polarization of electric field[23, 30]. Therefore, there exists an oscillating dipole at the two ends of the slit and the aperture array is equivalent to a dipole emitter array. The equivalent dipole emitter array radiates the scattered energy

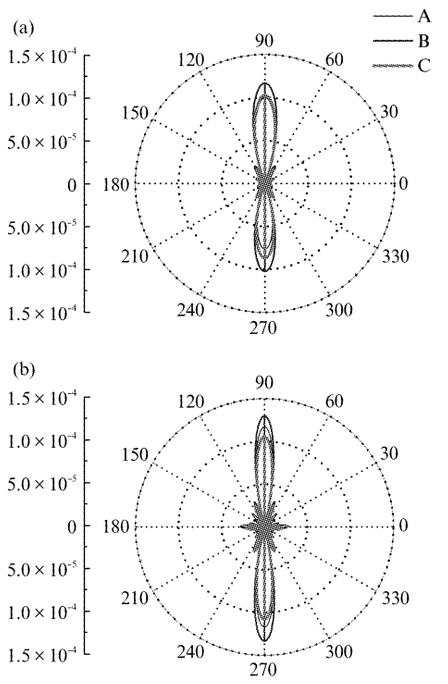

Fig. 3 (Color online) The calculated far-field E plane patterns for the arrays aperture array excited by TE incidence of sample A, B and C. (a) Far-field patterns in *yz* plane at the lower frequency 22.5, 20.5 and 20 THz, respectively, (b) far-field patterns in *yz* plane at the higher frequency 31, 28 and 28 THz, respectively

图3 样品A、B和C在TE光入射下的远场方向图仿真结果 (a)在22.5、20.5和20 Hz低频处在*yz*平面的远场方向图, (b)在31、28和28 Hz高频处在*yz*平面的远场方向图

into the far-field region. The resonant frequencies of the dipole are at the center of the HF and LF bands. Consequently, the antenna's SRIFs match the central positions of HF and LF bands basically.

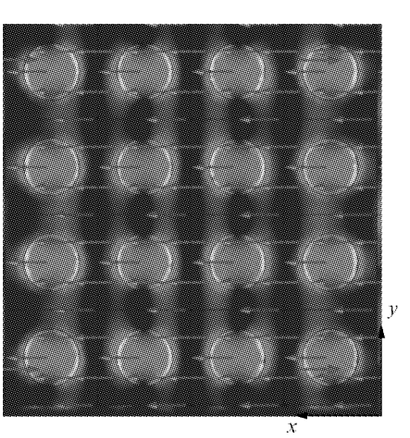

Fig. 4 The distribution of electric magnitude and the electric displacement vector (arrows) at the top silver layer

图4 上层银表面的电场分布图和电位移矢量图(图中箭头表示)

When the incident light illuminates the metallic aperture array, both SPP modes and LSP modes will be ex-

cited[33]. The HF band and LF band are due to the excitations of both the SPP modes and the LSP modes. SPPs will be excited when their momentum matches the momentum of the incidence and the periodic structure as follows[28]:

$$\vec{k}_{sp} = \vec{k}_x \pm \vec{G}_{pq} \quad , \quad (1)$$

where $|k_{sp}| = |2\pi f_{sp}/c| \sqrt{\frac{\varepsilon_1\varepsilon_2}{(\varepsilon_1+\varepsilon_2)}}$ is the wave vector of the SPP, ε_1 and ε_2 are the relative dielectric constant of the two adjacent dielectrics, $|k_x| = (2\pi f_{sp}/c)\sin\theta$ is the incident plane wave vector. $|G_{pq}| = 2\pi/n$ is the periodic structure momentum and n is the lattice constant. At the normal incidence, $k_x = 0$, then equation (1) can be simplified as follows:

$$f_{sp} = \frac{c}{\left(n\sqrt{\frac{\varepsilon_1\varepsilon_2}{(\varepsilon_1+\varepsilon_2)}}\right)} \quad , \quad (2)$$

where f_{sp} is the frequency of the excited SPP mode for the periodic structure. The HF band is excited by the Air/Ag SPP modes. The calculated Air/Ag (1, 0) SPP modes of samples A, B and C is 33.33, 29.99 and 29.99 THz, respectively, close to the experimental ones (31.15, 27.82 and 27.82 THz). The LF band is excited by the Ag/SU－8 SPP modes. The calculated Ag/SU－8 (1,0) SPP modes calculated for samples A, B and C is 20.83, 18.75 and 18.75 THz, respectively, close to the experimental ones (23.44, 21.58 and 21.52 THz). Besides the excitation of SPP modes, the positions of the HF and LF bands are also related to the excitation of LSP modes. The frequency of LSP mode for one circular waveguide can be expressed as follows[34]:

$$f = \frac{1.841}{(2\pi R)} \quad , \quad (3)$$

where R is the radius of the metallic apertures. The calculated frequency of the LSP modes of samples A, B and C is at 35.29, 35.29 and 29.13 THz, respectively. Therefore, the positions of the HF and LF bands depend on both the lattice constant and the aperture diameter. The transmission band will redshift when the lattice constant increases or the aperture diameter increases. As the antenna's SRIFs match the central position of HF and LF bands, the SRIFs will redshift as the transmission band redshift.

When the absolute size of aperture decreases or the absolute lattice constant increases, the relative aperture size is decreased and the LSP mode becomes stronger[35]. Excited mainly by the LSP modes, the plasmon antennas' radiation intensity will increase as the LSP modes increase. Therefore, the transmission decrease and the plasmon antennas' radiation intensity increase when the aperture diameter decreases with a fixed lattice constant or the lattice constant increases with a fixed aperture diameter.

4 Conclusions

In summary, we have studied the transmission spectra and far-field radiation patterns of the periodic metallic arrays. Two transmission bands (HF band and LF band) were observed in mid-infrared region. The periodic metallic arrays can behave as electrical dipole arrays at the transmission peak when excited by plane wave. The intensity of the far-field radiation pattern increase with the decrement of the hole-diameter or the increment of the lattice constant. This work provides a unique way to design optical antennas. Our research results are useful in the design of novel light-emitting devices and mid-infrared sensors.

References

[1] Olmon R L, Krenz P M, Jones A C, *et al*. Near-field imaging of optical antenna modes in the mid-infrared[J]. *Optics Express*, 2008, **16**(25): 20295－20305.

[2] Alaverdyan Y, Sepúlveda B, Eurenius L, *et al*. Optical antennas based on coupled nanoholes in thin metal films[J]. *Nature Physics*, 2007, **3**(12): 884－889.

[3] Reichenbach P, Eng L M, Georgi U, *et al*. 3D-steering and superfocusing of second-harmonic radiation through plasmonic nano antenna arrays[J]. *Journal of Laser Applications*, 2012, **24**: 042005.

[4] Kawata S, Ono A, Verma P. Subwavelength colour imaging with a metallic nanolens[J]. *Nature Photonics*, 2008, **2**(7): 438－442.

[5] Zhou L, Gan Q, Bartoli F J, *et al*. Direct near-field optical imaging of UV bowtie nanoantennas[J]. *Optics Express*, 2009, **17**(22): 20301－20306.

[6] Greffet J J. Nanoantennas for light emission[J]. *Science*, 2005, **308**(5728): 1561－1563.

[7] Alda J, Rico-García J M, López-Alonso J M, *et al*. Optical antennas for nano-photonic applications[J]. *Nanotechnology*, 2005, **16**(5): S230.

[8] Maraghechi P, Elezzabi A Y. Experimental confirmation of design techniques for effective bow-tie antenna lengths at THz frequencies [J]. *Journal of Infrared, Millimeter, and Terahertz Waves*, 2011, **32**(7): 897－901.

[9] Schuck P J, Fromm D P, Sundaramurthy A, *et al*. Improving the mismatch between light and nanoscale objects with gold bowtie nanoantennas[J]. *Physical Review Letters*, 2005, **94**(1): 017402.

[10] Dregely D, Taubert R, Dorfmüller J, *et al*. 3D optical Yagi-Uda nanoantenna array[J]. *Nature communications*, 2011, **2**: 267.

[11] Taminiau T H, Stefani F D, van Hulst N F. Enhanced directional excitation and emission of single emitters by a nano-optical Yagi-Uda antenna[J]. *Opt. Express*, 2008, **16**(14): 10858－6.

[12] Li J, Salandrino A, Engheta N. Optical spectrometer at the nanoscale using optical Yagi-Uda nanoantennas[J]. *Physical Review B*, 2009, **79**(19): 195104.

[13] Gao H, Shi H, Wang C, *et al*. Surface plasmon polariton propagation and combination in Y-shaped metallic channels[J]. *Optics Express*, 2005, **13**(26): 10795－10800.

[14] Pavlov R, Curto A G, van Hulst N F. Log-periodic optical antennas with broadband directivity[J]. *Optics Communications*, 2012.

[15] Liu Y G, Li Y, Sha W E I. Directional far-field response of a spherical nanoantenna[J]. *Optics letters*, 2011, **36**(11): 2146－2148.

[16] Bonod N, Devilez A, Rolly B, *et al*. Ultracompact and unidirectional metallic antennas[J]. *Physical Review B*, 2010, **82**(11): 115429.

[17] Lereu A L, Sanchez - Mosteiro G, Ghenuche P, *et al*. Individual gold dimers investigated by far - and near - field imaging[J]. *Journal of microscopy*, 2008, **229**(2): 254－258.

[18] Girard J, Scherrer G, Cattoni A, *et al*. Far-field optical control of a movable subdiffraction light grid[J]. *Physical review letters*, 2012, **109**(18): 187404.

[19] Wenger J, Gérard D, Dintinger J, *et al*. Emission and excitation contributions to enhanced single molecule fluorescence by gold nanometric apertures[J]. *Opt. Express*, 2008, **16**(5): 3008－3020.

[20] Wang X D, Ye Y H, Ma J, *et al*. Influence of filling medium of holes on the negative-index response of sandwiched metamaterials[J]. *Chi-*

nese Physics Letters, 2010, **27**(9): 094101.
[21] Hicks E M, Zhang X, Zou S, *et al*. Plasmonic properties of film over nanowell surfaces fabricated by nanosphere lithography[J]. *The Journal of Physical Chemistry B*, 2005, **109**(47): 22351-22358.
[22] Pang Y, Genet C, Ebbesen T W. Optical transmission through subwavelength slit apertures in metallic films[J]. *Optics Communications*, 2007, **280**(1): 10-15.
[23] Shi X, Hesselink L, Thornton R L. Ultrahigh light transmission through a C-shaped nanoaperture[J]. *Optics letters*, 2003, **28**(15): 1320-1322.
[24] Fan W, Zhang S, Minhas B, *et al*. Enhanced infrared transmission through subwavelength coaxial metallic arrays[J]. *Physical review letters*, 2005, **94**(3): 033902.
[25] Ebbesen T W, Lezec H J, Ghaemi H F, *et al*. Extraordinary optical transmission through sub-wavelength hole arrays[J]. *Nature*, 1998, **391**(6668): 667-669.
[26] Xu H, Zhu P, Craighead H G, *et al*. Resonantly enhanced transmission of light through subwavelength apertures with dielectric filling [J]. *Optics Communications*, 2009, **282**(7): 1467-1471.
[27] Tang Z H, Peng R W, Wang Z, *et al*. Coupling of surface plasmons in nanostructured metal/dielectric multilayers with subwavelength hole arrays[J]. *Physical Review B*, 2007, **76**(19), 195405.
[28] Guo H, Meyrath T P, Zentgraf T, *et al*. Optical resonances of bowtie slot antennas and their geometry and material dependence[J]. *Optics express*, 2008, **16**(11): 7756-7766.
[29] Wu Y M, Li L W, Liu B. Gold bow-tie shaped aperture nanoantenna: Wide band near-field resonance and far-field radiation[J]. *Magnetics, IEEE Transactions on*, 2010, **46**(6): 1918-1921.
[30] Turkmen M, Aksu S, ? etin A E, *et al*. Multi-resonant metamaterials based on UT-shaped nano-aperture antennas[J]. *Optics Express*, 2011, **19**(8): 7921-7928.
[31] Zhang Z J, Peng R W, Wang Z, *et al*. Plasmonic antenna array at optical frequency made by nanoapertures[J]. *Applied Physics Letters*, 2008, **93**(17): 171110-171110-3.
[32] Wang X, Ye Y H, Zheng C, *et al*. Tunable figure of merit for a negative-index metamaterial with a sandwich configuration[J]. *Optics letters*, 2009, **34**(22): 3568-3570.
[33] Johnson P B, Christy R W. Optical constants of the noble metals[J]. *Physical Review B*, 1972, **6**(12): 4370.
[34] Baida F I, Belkhir A, Van Labeke D, *et al*. Subwavelength metallic coaxial waveguides in the optical range: Role of the plasmonic modes [J]. *Physical Review B*, 2006, **74**(20): 205419.
[35] Degiron A, Lezec H J, Yamamoto N, *et al*. Optical transmission properties of a single subwavelength aperture in a real metal[J]. *Optics Communications*, 2004, **239**(1): 61-66.